atmosphere

MDPI

Article

Conversion Coefficient Analysis and Evaporation Dataset Reconstruction for Two Typical Evaporation Pan Types—A Study in the Yangtze River Basin, China

Ziheng Li, Xuefeng Sang *, Siqi Zhang, Yang Zheng and Qiming Lei

State Key Laboratory of Simulation and Regulation of Water Cycle in River Basin, China Institute of Water Resources and Hydropower Research, Beijing 100038, China
* Correspondence: sangxf@iwhr.com

Abstract: For the day-by-day evaporation observation data in the Yangtze River Basin from 1951 to 2019, the effects of the gradual shift of observation instruments from 20 cm diameter evaporation pan (D20) to E601 evaporation pan after 1980 are discussed, including inconsistent data series, and missing and anomalous data. This study proposes a governance and improvement method for dual-source evaporation data (GIME). The method can accomplish the homogenization of data from different observation series and solve the problem of inconsistent and missing data, and we applied it in practice on data of the Yangtze River Basin. Firstly, the primary and secondary periods of the data were obtained by wavelet periodicity analysis; secondly, we considered the first cycle of observations to be representative of the sample and calculated the conversion relationship between the primary and secondary periods; thirdly, the conversion coefficient between the dual-source observations was calculated, and the results were corrected for stations outside the main cycle; finally, the daily evaporation dataset of E601 pan was established through data fusion and interpolation technology. The study found that the annual average conversion coefficients of the D20 and E601 pans in the Yangtze River Basin are basically between 0.55 and 0.80, and there are obvious differences in different regions. The conversion coefficient is positively correlated with relative humidity, wind speed, minimum temperature and altitude; and negatively correlated with sunshine duration, average temperature and maximum temperature. Evaporation is high in the upper reaches of the basin and low in the middle and lower reaches; in particular, evaporation is highest in the southwest, which is associated with the drought hazards. In addition, the article presents the spatial distribution of the conversion coefficients of D20 and E601 pans in the Yangtze River Basin. The results can realize the rapid correction of the evaporation data of the local meteorological department, and can be extended to the processing of other types of data in similar areas.

Keywords: conversion coefficients; evaporation; 20 cm diameter pan; E601 pan; wavelet analysis; Yangtze River Basin

check for updates

Citation: Li, Z.; Sang, X.; Zhang, S.; Zheng, Y.; Lei, Q. Conversion Coefficient Analysis and Evaporation Dataset Reconstruction for Two Typical Evaporation Pan Types—A Study in the Yangtze River Basin, China. *Atmosphere* **2022**, *13*, 1322. https://doi.org/10.3390/atmos13081322

Academic Editors: Zhibin Sun, Yan-An Liu and Zigang Wei

Received: 3 July 2022
Accepted: 16 August 2022
Published: 19 August 2022

Publisher's Note: MDPI stays neutral with regard to jurisdictional claims in published maps and institutional affiliations.

Copyright: © 2022 by the authors. Licensee MDPI, Basel, Switzerland. This article is an open access article distributed under the terms and conditions of the Creative Commons Attribution (CC BY) license (https://creativecommons.org/licenses/by/4.0/).

1. Introduction

Evaporation is an important component of the surface heat balance and an important link in the water vapor balance, and it plays a pivotal role in the global water cycle and climate evolution [1,2]. Since it incorporates the effects of climate variables on terrestrial evapotranspiration, pan evaporation has grown in importance as a physical indicator to measure atmospheric evaporative demand [3–5]. It is frequently used in irrigation scheduling, water balance, sustainable water management and hydrological modeling. Thus, observation networks of pan evaporation have been established and maintained across the globe [6–8].

Due to the use of different types of 20 cm diameter (D20) and E601 pans (Figure 1 and Table 1), the observed pan data in China are discontinuous and inconsistent across the

global network of evaporation pan observations. The observation of pan evaporation at hydrological stations in China started in the 1920s [9]; among them, the D20 pan observation began in 1950, and these data have good continuity and are of great value to China's climate research. However, because it is installed at a height of 70 cm from the ground, the volume is small and the walls of the vessel are exposed to the air, it cannot represent the actual evaporation of the place, and it was gradually replaced after 2001.

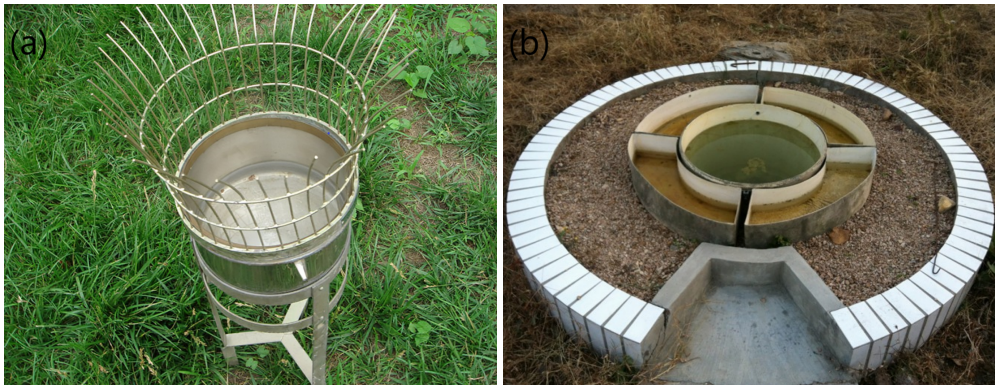


Figure 1. Two types of evaporation pans: 20 cm diameter evaporation pan (**a**); E601 evaporation pan (**b**).

Table 1. Detailed information on the two types of evaporation pans.

Name of Evaporimeter	Size	Description
D20	Area: 314 cm^2 (diameter: 20 cm) Depth: 10 cm	Rim is 70 cm from the ground, in every meteorological station in China
E601	Area: 3000 cm^2 Depth: 60 cm (cylinder) C + 8.7 cm (circular cone)	fiberglass material, surrounded by water and soil circle. Installed in every meteorological station from 1998

After 1980, China installed the E601 pan bit by bit, and its evaporation volume is close to the actual evaporation volumes of small and medium-sized water bodies, such as lakes and reservoirs [10,11]. However, in practice, it was found that the E601 pan suffers freezing problems in the winter; thus, D20 was kept or re-deployed in some regions [12]. The nationwide evaporimeter replacement and the D20 pan's reuse in certain regions or months each year make it impossible to utilize evaporation pan measurements from China to estimate long-term changes in atmospheric evaporative demand [13–15].

In recent years, the global climate system has experienced significant changes characterized by warming, and with the release of the IPCC Special Report on Global Warming of 1.5 °C by the Intergovernmental Panel on Climate Change (IPCC) in Incheon, South Korea on 8 October 2018 [16], changes in climate conditions can no longer be ignored. The Yangtze River Basin is the largest water resource zone in China and has an extremely complex water cycle system. Evapotranspiration as a dissipation factor is an important influence on the water cycle and water resources' development and utilization. Faced with discontinuous and inconsistent evaporation data, it was necessary to carry out data governance and enhancement work on both types of data and to construct a continuous water surface evaporation series that could be used for hydrological analysis.

Many scholars have studied the estimation method of evapotranspiration [17–20]. A simple evaporation model for evaporation pan is proposed and can be used to analyze monthly average yields from the Global Climate Model (GCM), and we demonstrated that this will be a valuable tool to reconcile observations of pan evaporation trends with climate model simulations [21]. The surface evaporation data collected in the past were

merged with the latest data collected by automatic weather stations, and a complete dataset of evaporation from large evaporation pans was constructed using a second-generation statistical regression technique (partial least squares) based on evaporation observations from large and small pans [22]. Using the Penman Monteith method, reference crop evapotranspiration was calculated for 46 meteorological stations in the Yangtze River Delta region from 1957 to 2014, and its spatial distribution and temporal trends were studied [23]. Based on the the homogenization and interpolation of meteorological data and the assimilation of evaporation from evaporation pans, a continuous and consistent month-by-month 0.05° reanalysis dataset was established for the D20 and 601B flat areas of mainland China from 1960 to 2014 [24].

The interrelationship between the evaporation pan and the actual evaporation is also of interest. In the Northwest Dry Early Zone, hourly evaporation was measured with E601B, Class A and D20 evaporated blood, and local actual evaporation was measured with an eddy correlation system. The results showed that with changes in ambient humidity, the actual daily evaporation showed a contradictory trend to the evaporation rate of the evaporated pan, and the relationship between the two evaporation rates showed clear asymmetric complementary behavior [25]. The potential evaporation calculated using the Penman method (based on the Monin–Obukhov similarity theory and based on the Roman wind function) and the evaporation obtained from evaporation trays (D20 evaporation pan and E601B pan) were chosen, and the differences between the four formulations in estimating the actual evaporation were compared using the generalized complementary function [12].

In addition, many other scholars have studied the conversion coefficients of D20 and E601 pans [26,27]. The conversion coefficients of free water surface evaporation were investigated. Comparisons were made between numerous evaporation tanks (pans) and a 20 m^2 evaporation tank [28]. Sheng [29] analyzed the distribution pattern of the conversion coefficients between the D20 pan and theoretically calculated water surface evaporation, and established a regression model of the annual average conversion coefficient and each meteorological element applicable to the whole country. To fully use the records from the two pans and obtain long-term pan evaporation, the spatial patterns of conversion coefficients between D20 and E601 and the factors that influence conversion coefficients were investigated based on records from 573 national meteorological stations from 1998 to 2001 [30].

Based on the evaporation data of D20 and E601 pans from meteorological stations in the Yangtze River Basin from 1951 to 2019, we used the governance and improvement method for dual-source evaporation data (GIME) and Morlet wavelet analysis theory to extract the evaporation data with completeness, series representation and time-series consistency. The conversion coefficients between the two types of pans were calculated, and the distribution patterns of the conversion coefficients of the two evaporation sources in the Yangtze River Basin were analyzed. Ultimately, the daily dataset of the E601 evaporation pan was constructed to provide a reasonable basis for the effective and complete use of a long series of evaporation hydrological data from the Yangtze River Basin.

2. Materials

2.1. Study Area

The Yangtze River Basin lies between 90°33′–122°19′ E and 24°27′–35°54′ N. It has a narrow shape: short north–south and long east–west. It is bounded in the north by the Qinling Mountains; in the northeast by the Funiu Mountains, the Tongbai Mountains and the Dabie Mountains and the Yellow River Basin; and in the south by the Nanling Mountains, the Qianzhong Plateau, the Dayu Mountains, the Wuyi Mountains and the Tianmu Mountains and the Pearl River Basin and the Min and Zhejiang water basins. Most of the basin has a subtropical monsoon climate, mainly comprising the Indian summer monsoon, which controls the upper regions, and the East Asian summer monsoon, which affects the middle and lower regions. The geography and topography of the basin are

complex and varied, and the climate varies significantly from place to place. The part of the basin that originates on the Qinghai–Tibet Plateau has a highland mountainous climate, and the annual mean temperature tends to be high in the east and low in the west, and high in the south and low in the north, due to the combined influence of solar energy, the East Asian atmospheric circulation, the large topography of the Qinghai–Tibet Plateau and the North Pacific Ocean, and the different topographic conditions of each region.

2.2. Data Acquisition

The data used are national meteorological station data, from which we selected 300 meteorological stations in and around the Yangtze River Basin (Figure 2). The data are day-by-day observations of the D20 and E601 evaporation pans. The long series of data from the two evaporation pans suffer from inconsistent measurement standards, significant inconsistency of data, missing fragments of data and anomalies. The data series of D20 pan basically cover 1951–2001, and the data series of E601 pan basically cover 1979–2019.

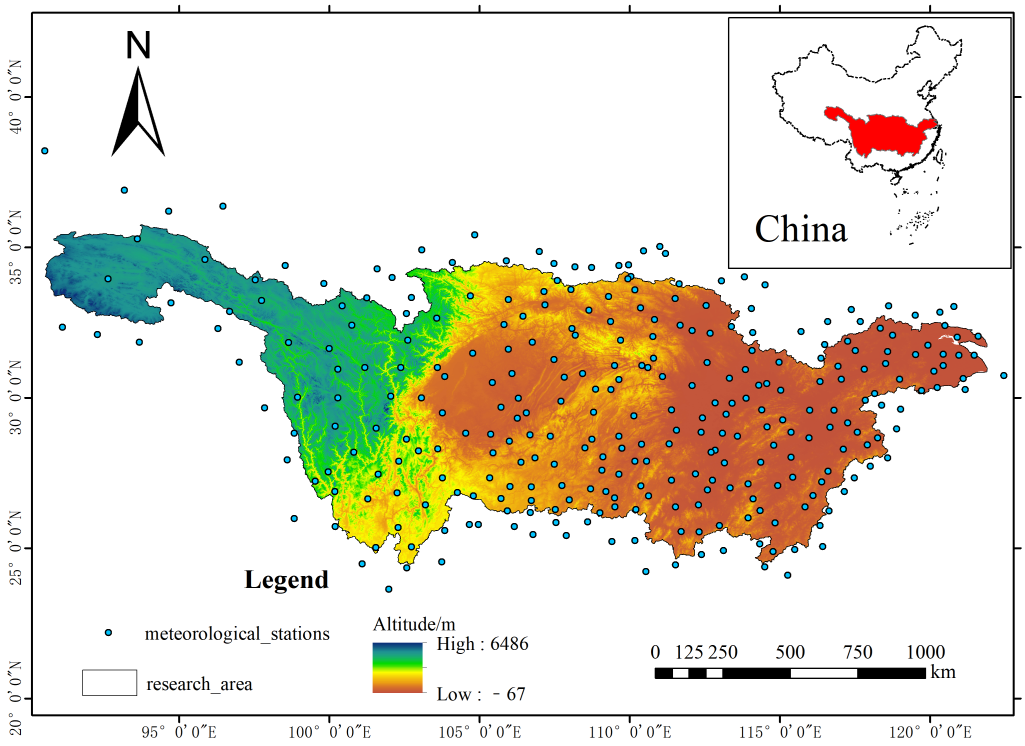


Figure 2. Distribution of meteorological stations in the Yangtze River Basin.

3. Methods

This paper proposes a governance and improvement method for dual-source evaporation data (GIME). It uses Morlet wavelet analysis theory and the conversion coefficient of the two evaporation data as a bridge; its goal is to integrate the dual-source dataset into a single-source dataset. GIME was the main framework of the research methodology, and wavelet analysis was used as a representative discriminant for the data series; see Section 3.2 for GIME. During the pre-data review, it was found that there were some missing data for both evaporation data, and a large difference in the lengths of the overlapping series of dual-source evaporation data used to calculate the conversion coefficient, which resulted in inconsistent data and unreliable results. Therefore, data cleaning and extraction were required to determine the completeness and representativeness of the calculated site data prior to the calculation of the conversion coefficient.

Firstly, the completeness of the annual data was determined by the dual-source dataset completeness matrix (see Section 3.2.2 for details), and the complete data series of each site was taken out; secondly, the data were homogenized and analyzed, and since the data series

of the D20 evaporation pan was longer than that of E601, the long series of D20 evaporation data was selected and wavelet periodicity analysis was performed to determine the primary and secondary periods, which were used as the dual-source evaporation overlap series length discriminators, dividing the station observations that satisfy different cycles (see Section 3.2.3 for details). Afterwards, data fusion was performed to integrate the dual-source dataset into a single-source dataset (see Section 3.2.4 for details). Subsequently, various methods, such as site data interpolation and nearby site correction transplantation, were used to improve the missing fragment data in the dataset (see Section 3.2.5 for details). Finally, the reconstruction of the daily evaporation dataset for the E601 pan was achieved. The methodological process (Figure 3) and the practical application steps (Figure 4) are as follows.

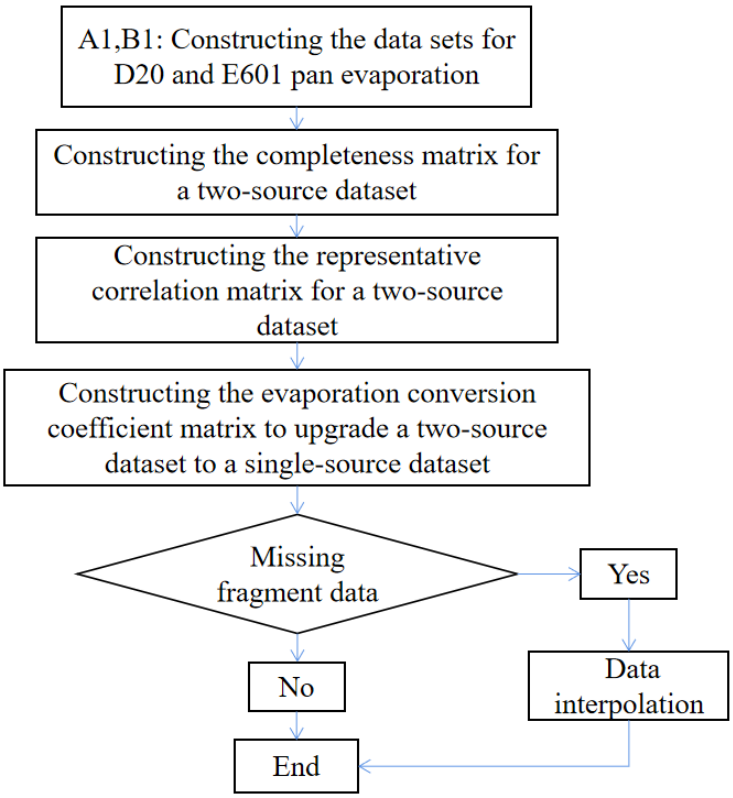


Figure 3. Governance and improvement method process for dual-source evaporation data.

3.1. Morlet Wavelet Analysis

Wavelet analysis is an effective method with which to process image signals and time series data [31]. It can also be applied to geographic research, since various geographic phenomena can be regarded as signals that change periodically [32]. In this paper, Morlet wavelets are used to reveal the period of multiscale variability in a long series of evaporative pan observations. Information on wavelet analysis applications can be found in previous studies [33,34].

The wavelet basis functions are expressed here:

$$\psi_{a,b}(t) = |a|^{-1/2}\psi\left(\frac{t-b}{a}\right) \quad (1)$$

In the above formula, $a, b \in \mathrm{R}, a \neq 0$. $\psi_{a,b}(t)$ is the wavelet basis function; a represents the time scale, which reflects the length of the wavelet period; b is the translation parameter, which reflects the passage of the wavelet in time.

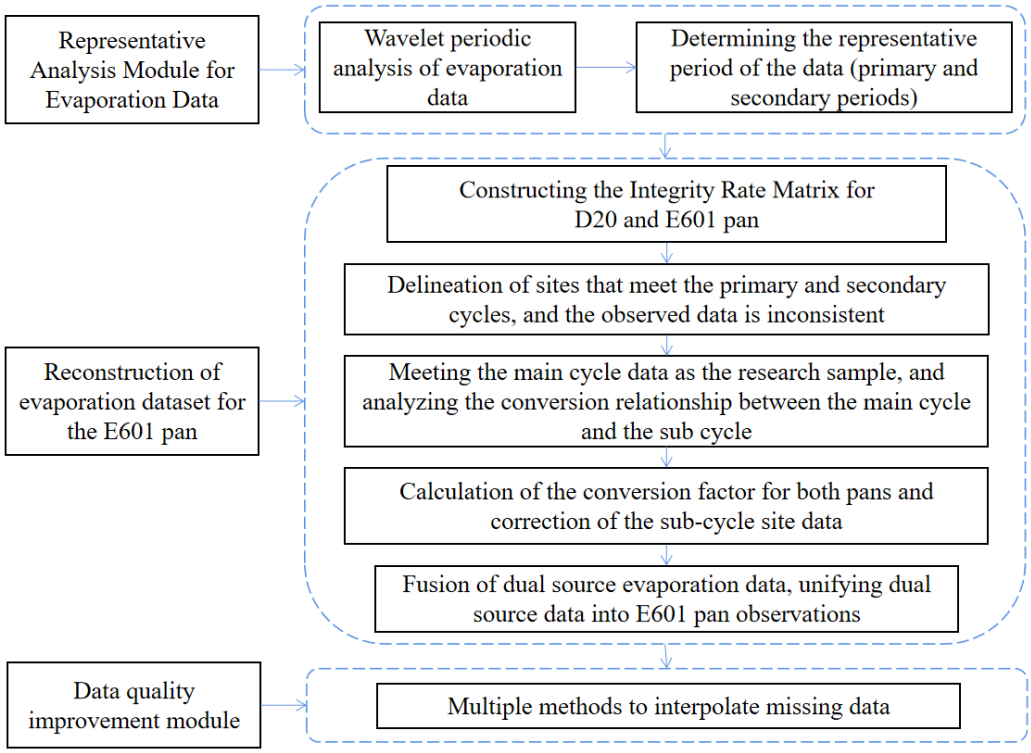


Figure 4. Practical application steps of governance and improvement method for dual-source evaporation data.

The continuous wavelet transform (CWT) is as follows:

$$W_f(a,b) = |a|^{-1/2} \int_R f(t)\bar{\psi}\left(\frac{t-b}{a}\right)dt \tag{2}$$

In the above formula, $W_f(a,b)$ is the wavelet transform coefficient; $f(t)$ is a finite signal; $\bar{\psi}\left(\frac{t-b}{a}\right)$ is the complex conjugate function of $\left(\frac{t-b}{a}\right)$.

The wavelet variance is calculated by integrating the square value of the wavelet coefficients in the domain. The formula is as follows:

$$\mathrm{Var(a)} = \int_{-\infty}^{\infty} \left|W_f(a,b)\right|^2 db \tag{3}$$

In the above formula, the wavelet variance graph is the curve of the wavelet variance, which is varied with the time scale a. The wavelet variance graph can be used to judge the relative intensity of the time series or signal vibration on different time scales, and the scale corresponding to the maximum value of variance is the fluctuation period of the time series.

3.2. Governance and Improvement Method for Dual-Source Evaporation Data

3.2.1. Construction of the Initial Dataset

The initial matrices A_1 and B_1 were constructed from the long series of evaporation data measured by the the D20 and E601 pans at the site.

$$\mathrm{A_1} = \begin{bmatrix} a_{111} & a_{112} & \cdots & a_{11j} \\ a_{121} & a_{122} & \cdots & a_{12j} \\ \vdots & \vdots & \ddots & \vdots \\ a_{ti1} & a_{ti2} & \cdots & a_{tij} \end{bmatrix} \tag{4}$$

$$\mathrm{B}_1 = \begin{bmatrix} b_{111} & b_{112} & \cdots & b_{11j} \\ b_{121} & b_{122} & \cdots & b_{12j} \\ \vdots & \vdots & \ddots & \vdots \\ b_{ti1} & b_{ti2} & \cdots & b_{tij} \end{bmatrix} \tag{5}$$

In the above formula, $a_{t,i,j}$ is the daily measurement of the E601 pan at site j on day i of year t, mm; $b_{t,i,j}$ is the daily measurement of the the D20 pan at site j on day i of year t, mm.

3.2.2. Construction of the Dataset Completeness Matrix

We constructed a completeness matrix C for the D20 and E601 pan evaporation data, and the years in which the annual data completeness rate reach $Z_{\max}$% were used for the evaporation conversion factor calculation (32,766 for outliers or missing data).

$$\mathrm{C} = \begin{bmatrix} C_{11} & C_{12} & \cdots & C_{1j} \\ C_{21} & C_{22} & \cdots & C_{2j} \\ \vdots & \vdots & \ddots & \vdots \\ C_{\mathrm{t1}} & C_{\mathrm{t2}} & \cdots & C_{\mathrm{tj}} \end{bmatrix} \tag{6}$$

$$c_{t,j} = \left(\sum_{1}^{y} k_{t,i,j} \right) / y * 100 \tag{7}$$

$$k_{t,i,j} = \begin{cases} 1, & a_{t,i,j} < 9999, b_{t,i,j} < 9999 \\ 0, & \text{otherwise} \end{cases} \tag{8}$$

In the above matrix, $c_{t,j}$ is the proportion of days in year t when measurements are available for the D20 and E601 pans at site j at the same time; $k_{t,i,j}$ is the discriminant value for the presence of measured data for the D20 and E601 pans at site j on day i of year t ; y is the number of days in a year, 366 days in leap years and 365 days for the rest.

3.2.3. Representative Correlation Matrix for the Dataset

After wavelet periodicity analysis to determine the first main period of the evaporation hydrological data series, X years, it can be considered that the calculation results of the continuous hydrological series of X years are representative. Therefore, it is necessary to calculate the evaporation commutation factor using the data series of the intersections of the evaporation datasets of the D20 and E601 pans for greater than X years, and construct the dataset representative correlation matrix D.

$$\mathrm{D} = \begin{bmatrix} d_{11} & d_{12} & \cdots & d_{1j} \\ d_{21} & d_{22} & \cdots & d_{2j} \\ d_{31} & d_{32} & \cdots & d_{3j} \end{bmatrix} \tag{9}$$

In the above matrix, $d_{1,j} = d_j$, $d_j = \max\left(\sum t_{t_1}^{t_2} W\right)$, d_j is the intersection length of the D20 or E601 pan evaporation datasets at site j and the given year; t_1 is the effective start year at site j; t_2 is the effective end year at site j; $d_{2,j} = t_1$, $d_{3,j} = t_2$; W = 1, this indicates that the evaporation data series is representative, and the data need to meet this condition: $c_{t1,j} > z_{\max}, c_{t1+1,j} > z_{\max}, c_{t1+2,j} > z_{\max} \cdots c_{t2,j} > z_{\max}$.

3.2.4. Construction of the Evaporation Conversion Coefficient Matrix

Formula for calculating the evaporation conversion coefficient:

$$Z = E_0 / E_1 \tag{10}$$

In the above formula, Z is the conversion coefficient; E_0 is the evaporation volume observed by the E601 pan, mm; E_1 is the evaporation volume observed by the D20 pan, mm.

Construction of the conversion coefficient matrix:

Sites with complete and representative data in the datasets were selected as eligible sites for calculating the evaporation conversion coefficients, and the conversion coefficient matrix was constructed according to the formula for calculating the conversion coefficients.

$$\mathrm{R} = \begin{bmatrix} r_{11} & r_{12} & \cdots & r_{1j} \\ r_{21} & r_{22} & \cdots & r_{2j} \\ \vdots & \vdots & \ddots & \vdots \\ r_{i1} & r_{i2} & \cdots & r_{ij} \end{bmatrix} \tag{11}$$

$$r_{i,j} = 1/d_{1j}\left(\sum_{d_{3j}}^{d_{2j}} a_{t,i,j}/b_{t,i,j}\right) \tag{12}$$

In the above formula, $r_{i,j}$ is the multi-year daily average of the evaporation conversion factor for day i at site j, mm; $a_{t,i,j}$ is the daily measurement of the E601 pan for matrix A1, mm; $b_{t,i,j}$ is the daily measurement of the D20 pan for matrix B1, mm; and $d_{1,j}$ and $d_{2,j}$, $d_{3,j}$ are the site parameters from the representative correlation matrix.

3.2.5. Reconstruction of the E601 Evaporation Pan Dataset

After reviewing the relevant literature, the E601 pan evaporation is more like the actual water surface evaporation of small and medium-sized water bodies such as lakes and reservoirs, so E601 pan data were chosen as the actual evaporation data, and D20 pan data were used as the supplementary values for the missing data of evaporation to construct the evaporation data matrix A_2.

$$\mathrm{A2} = \begin{bmatrix} a_{111} & a_{112} & \cdots & a_{11j} \\ a_{121} & a_{122} & \cdots & a_{12j} \\ \vdots & \vdots & \ddots & \vdots \\ a_{ti1} & a_{ti2} & \cdots & a_{tjj} \end{bmatrix} \tag{13}$$

$$a_{t,i,j}(\text{missing data}) = b_{t,i,j} * r_{i,j} \tag{14}$$

In the above matrix, $a_{t,i,j}$ is the daily measurement of the E601 pan at site j on day i of year t, mm; the original $a_{t,i,j}$ were retained, and the missing values of $a_{t,i,j}$ were replaced with $b_{t,i,j} * r_{i,j}$ to complete the assimilation of the datasets.

3.2.6. Interpolation of Missing Segments in the Dataset

Combining the evaporation dual source data may still have missing measurements for some periods, due to the absence of evaporation measurements for both evaporators. Therefore, two methods were considered for data quality enhancement: firstly, the multi-year daily average of the E601 pan was used to supplement the missing values; secondly, the fluctuation of the daily data of evaporation relative to its multi-year average from the E601 pan at the nearby station for that time period was chosen to correct the multi-year daily average of the station to supplement the missing values, and the time scale can be flexibly adjusted to 10 days, monthly, quarterly, etc.

The following calculation is an example, with matrix X1 being the E601 pan data and the missing data being a_{112}.

$$\mathrm{X1} = \begin{bmatrix} a_{111} & a_{112} & a_{113} \\ a_{121} & a_{122} & a_{123} \\ a_{131} & a_{132} & a_{133} \end{bmatrix} \tag{15}$$

In the above formula, $a_{t,i,j}$ is the daily measurement of the E601 pan at site j on day i of year t, mm.

Method 1: Multi-year daily averages of evaporation to supplement missing data,

This method is applicable to the upper Yangtze River Basin region, where meteorological stations are relatively sparse and missing data can be supplemented with multi-year averages from evaporation pans.

$$a_{122} = \frac{1}{n}\sum_{i=1}^{n} a_{1i2} \tag{16}$$

In the above formula, n is the length of the data series for the site and year.

Method 2: Construct a correction factor matrix and supplement missing data with corrections to multi-year daily averages.

When missing data are supplemented with multi-year daily averages, the accuracy of the data is deficient and does not take into account the effect of fluctuations in light, wind speed and sunlight on evaporation, so the quality of the data can be improved by using a corrected value of the multi-year daily average.

$$k = \frac{a_{121} + a_{123}}{\frac{1}{n}\sum_{i=1}^{n}(a_{1i1} + a_{1i3})} \tag{17}$$

$$a_{122} = \left(\frac{1}{n}\sum_{i=1}^{n} a_{1i2}\right) * k \tag{18}$$

In the above formula, k is a correction factor to calculate the fluctuation of the current year's observations at surrounding stations relative to the multi-year average.

4. Results and Discussion

4.1. Wavelet Periodicity Analysis of Evaporative Hydrological Series

Due to the inconsistent length of the evaporator observation data series at the meteorological stations, wavelet periodic analysis was used to determine the main and secondary periods of the long series of evaporation data, and to determine the minimum segment of the data time series length, in order to improve the representativeness and consistency of the observation data at each station later.

The long series of data measurements of the D20 pan in the Yangtze River Basin is relatively longer. After calculating the annual data completeness rate of evaporation from D20 pan, 25 stations with more complete data were selected for wavelet periodicity analysis, and the wavelet variance process lines of annual evaporation were obtained for 25 stations (Figure 5). Taking site 56093 as an example (Figure 6), firstly, the first, second and third peaks of the wavelet variance process line of the site were obtained as the first, second and third cycles of the annual evaporation variation of the site; secondly, frequency histograms were plotted, and the cycles of the long series evaporation data were obtained by fitting a normal distribution (Figure 7); finally, 23, 12 and 6 years were determined as the first, second and third cycles of the long series evaporation data of the Yangtze River Basin, respectively.

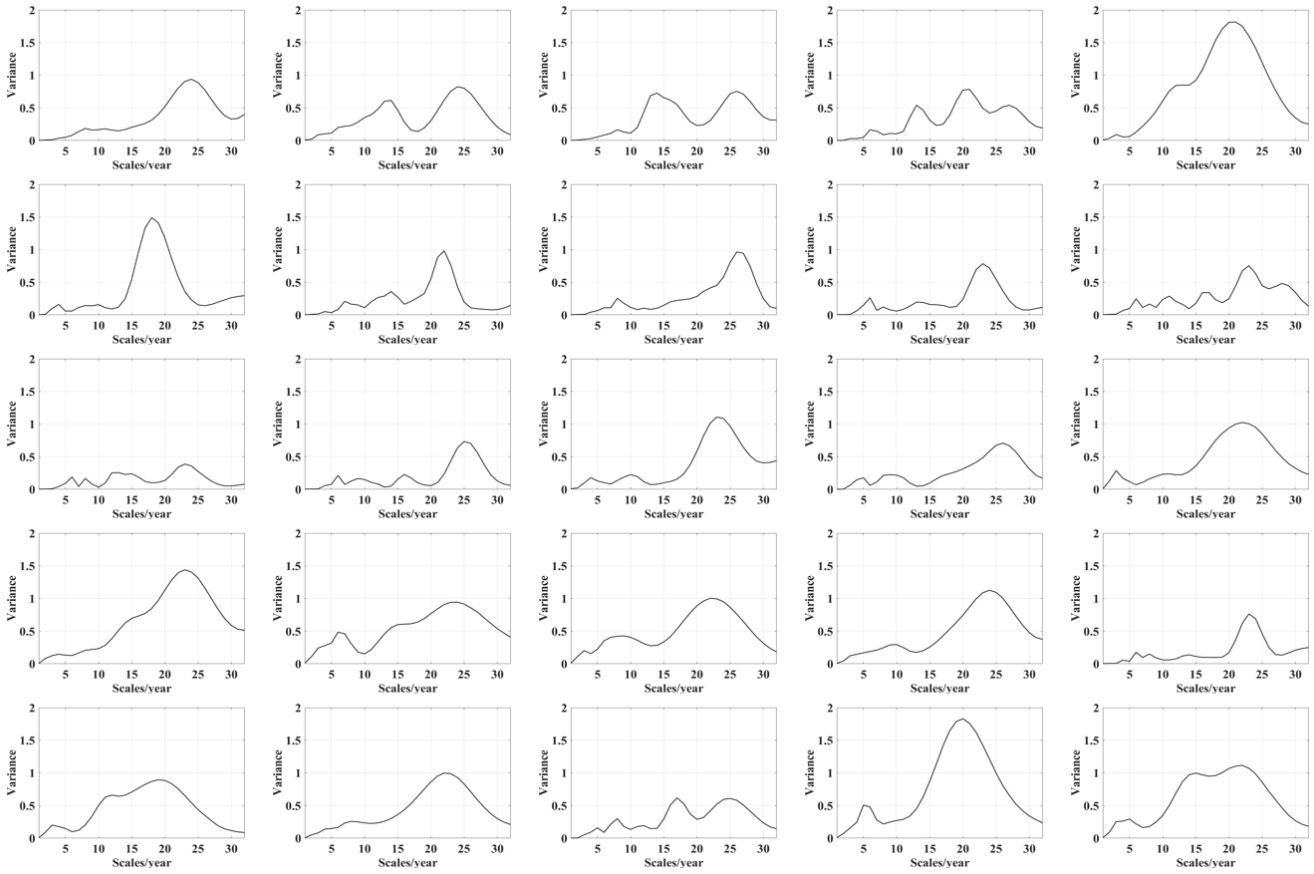


Figure 5. Wavelet variance of annual evaporation variation at 25 stations in the Yangtze River Basin.

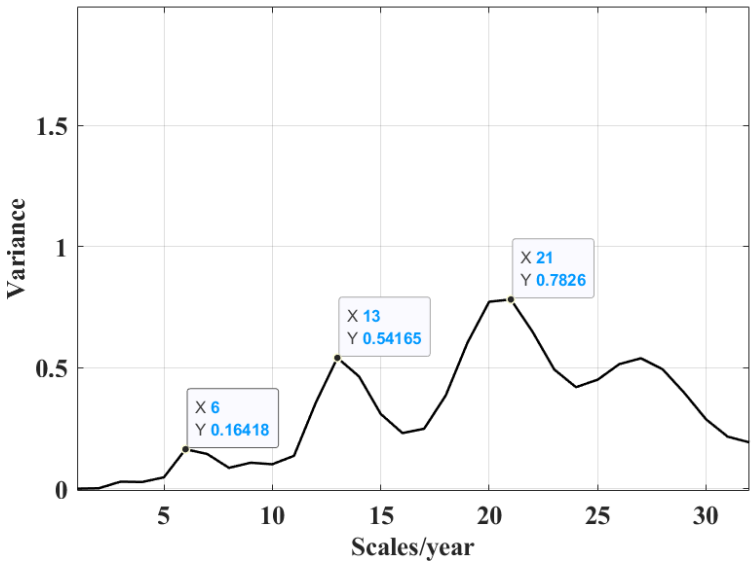


Figure 6. Variance diagram of wavelet analysis of annual evaporation at Station 56093 in the Yangtze River Basin.

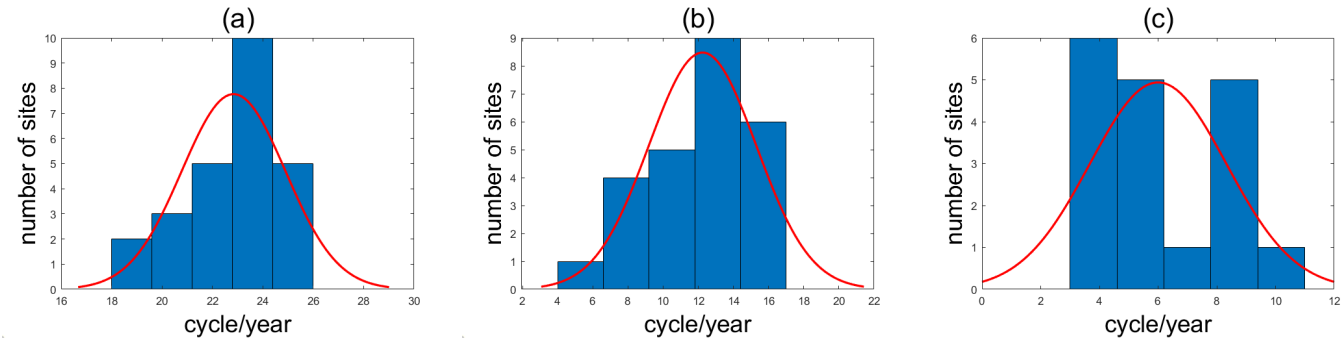


Figure 7. Frequency histograms of the first, second and third cycles of annual evaporation changes in the Yangtze River Basin, (**a**) first cycle, (**b**) second cycle and (**c**) third cycle.

4.2. Representative Analysis of Dual Source Evaporation Data

The observation data of D20 and E601 pans were counted, and the representativeness of the observation data of each station was analyzed according to the main and secondary cycles of the evaporation data, and the classification of representative stations at different levels was completed.

Based on the daily observation data of the D20 and E601 pans in the Yangtze River Basin, firstly, the missing annual measurement data of each station was obtained by constructing the completeness matrix of the station-evaporation data; secondly, the series length of the overlapping data of the two pans at each station was counted to construct the representative correlation matrix of the evaporation data (Table 2); finally, the first, second and third main cycles of the annual evaporation variation in the Yangtze River Basin were used to filter and classify the meteorological stations. There are 158 eligible stations: 25 stations covered in the first cycle (≥23 years), 31 stations covered in the second cycle (≥12 years) and 102 stations covered in the third cycle (≥6 years). In Figure 8, it can be seen that the representative dual-source evaporation data are basically distributed in the middle and lower reaches, which is due to the complex topography of the upper reaches of the Yangtze River Basin, which makes station construction more difficult.

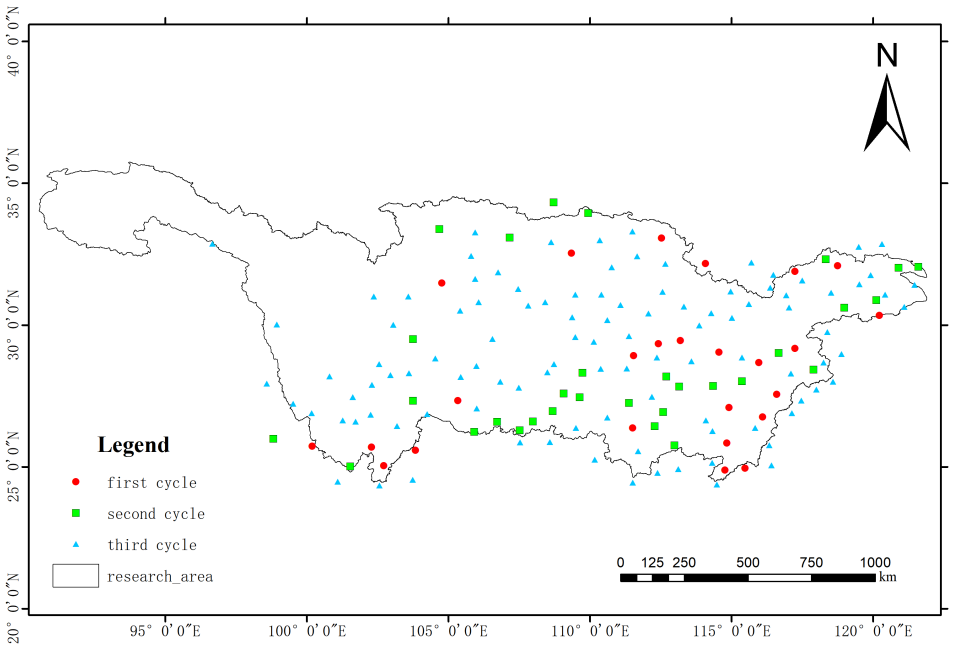


Figure 8. Distribution of stations corresponding to evaporation data meeting the first, second and third cycles.

Table 2. Representative correlation matrix of evaporation data for sites.

Site	Start Year	End Year	Data Length (Year)
57853	1992	2001	10
57866	1984	2001	18
57872	1986	2001	16
57874	1987	2001	15
57896	1964	1970	7
57902	1992	2001	10
57947	1997	2001	5
57972	1984	2001	18
57993	1984	2001	18
58122	1987	2001	15
58847	1980	2001	22

4.3. Calculation and Correction of Conversion Factors

Since meteorological station data can be divided into three period series, there is inconsistency in the calculation of the data from different series. We considered the first cycle (≥23 years) of observations to be representative of the sample as a whole and calculate the conversion relationship between the primary and secondary periods in this sample. The objective was to complete the homogenization of observations from the remaining stations that are under-represented.

Firstly, we selected 25 stations in the first cycle, selected the daily data of D20 and E601 pans from 1983 to 2005 (23 years), considered the data to be representative of the sample and calculated the conversion coefficients of the annual average evaporation of the two pans (Figure 9).

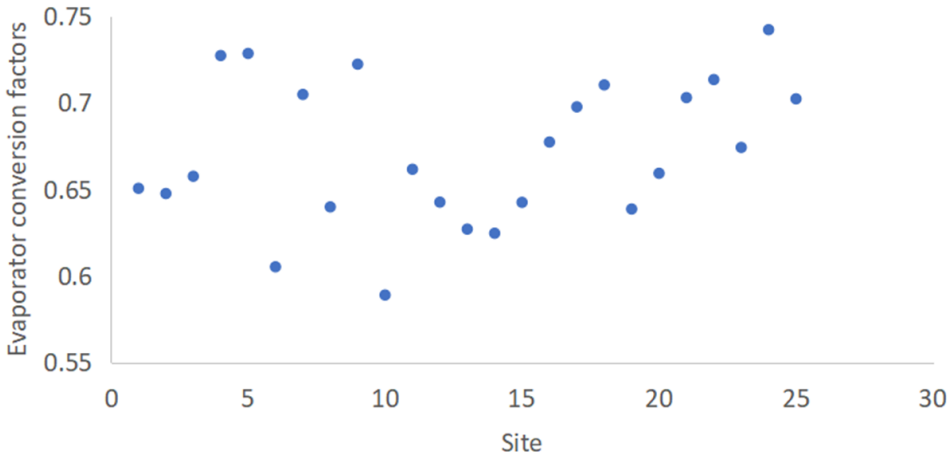


Figure 9. Conversion coefficients for two evaporation pans for the first cycle (series length of 23 years). The conversion coefficient is the observed value of E601 pan/D20 pan, and the formula used was Formula (10).

Secondly, for the 25 stations of the first cycle (series length of 23 years), the mean values of the conversion coefficients of the annual evaporation of the two pans were calculated every twelve years, using 1983 and 1994 as the starting years, 12 years of the second cycle as the calculation segment and 1994–2005 as the ending year, to construct a matrix of the conversion coefficients of the two pans of the second cycle (Figure 10).

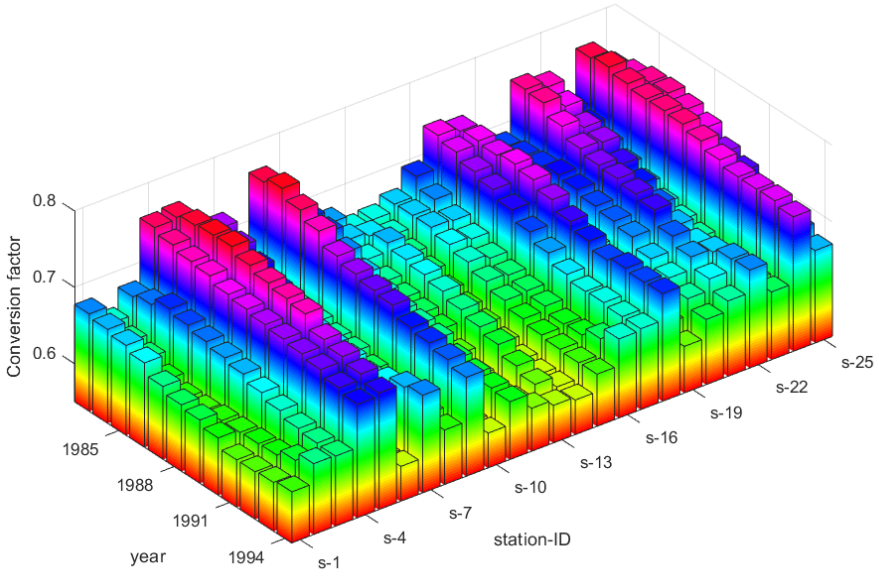


Figure 10. Matrix of conversion coefficients for two pans for the second cycle (series length of 12 years.

Next, the correction value (23-year inter-pan conversion factor/12-year inter-pan conversion factor) for the conversion factor transfer from the second sub-cycle (12 years) to the first main cycle (23 years) was calculated, and a correction factor matrix was constructed (Figure 11). The mean value of the correction factor matrix was taken as the correction value for the two pan commutation factors under the second sub-cycle, and the result was calculated to be 1.00427. This calculation improved the consistency of site data for both primary and secondary cycles.

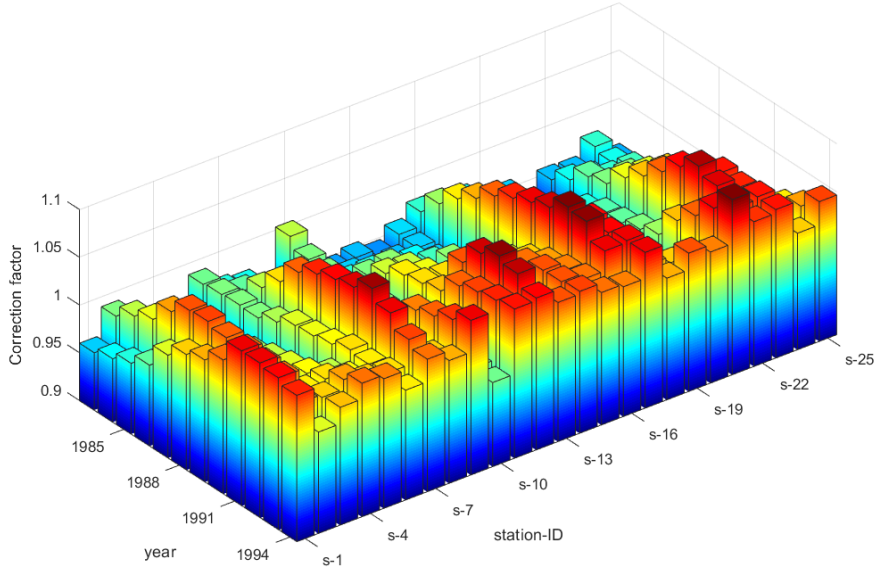


Figure 11. Correction factor matrix for the conversion of the second sub-cycle (12 years) to the first main cycle (23 years).

Thirdly, for the 25 stations of the first cycle (series length of 23 years), the mean values of the evaporation conversion factors for the two pans were calculated every six years, using 1983 and 2000 as the starting years, 6 years of the third cycle as the calculation

segment and 1988 and 2005 as the ending years, to construct a matrix of the conversion factors for the two pans for the third cycle (Figure 12).

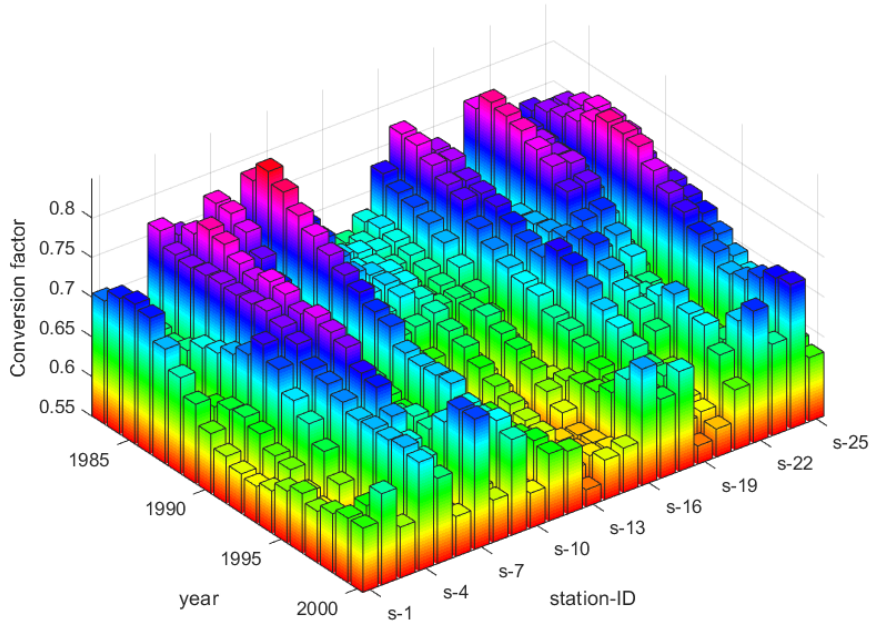


Figure 12. Matrix of conversion coefficients for two pans for the third cycle (series length of 6 years).

After that, the correction value (23 years conversion factor/6 years conversion factor) of the conversion factor from the third sub-cycle (6 years) to the first main cycle (23 years) was calculated to construct the correction factor matrix (Figure 13); the mean value of the correction factor matrix was taken as the correction value of the conversion factor of the two pans under the third sub-cycle and the result was calculated as 1.00564.

Finally, based on the above calculations, the correction values of the conversion factors of the two pans under the second and third sub-periods were used to correct the conversion factors of the D20 and E601 pans calculated at 133 meteorological stations outside the first period, so as to obtain the conversion coefficients between the observations of the two pans at 158 stations representative of the Yangtze River Basin.

After the above calculation process, we found that the volatility of the conversion coefficients of the two pans calculated in the third cycle (6 years) is more significant than that in the second cycle (12 years), indicating that on the time scale, the shorter series of measured data will reduce the representation of the data. Most long-term climatological time series are affected by several non-climatic factors that make these data unrepresentative of the actual climate variation occurring over time [35]. These factors include instrument replacement, geographical location of stations, observation methods and calculation methods. Xu [3] used the penalized maximum t test combined with a quantile matching method to homogenize the time series of daily maximum and minimum temperatures recorded at 825 stations in China from 1951 to 2010. Peter [36] proposed a homogenization method for time series comparison embedded in climate time series homogenization networks, which improves homogenization accuracy when the data contains synchronous breaks and semi-synchronous breaks. We carried out data mining from the perspective of data representation; statistical analysis of discontinuous and inconsistent dual-source evaporation data; and combined wavelet periodicity analysis to homogenize the data according to primary and secondary cycles. This was similar to the time series comparison method proposed by Peter, but for a different purpose, as in the latter, the time series comparison method is used to remove site effects, whereas we addressed the problem of inconsistent time series across sites.

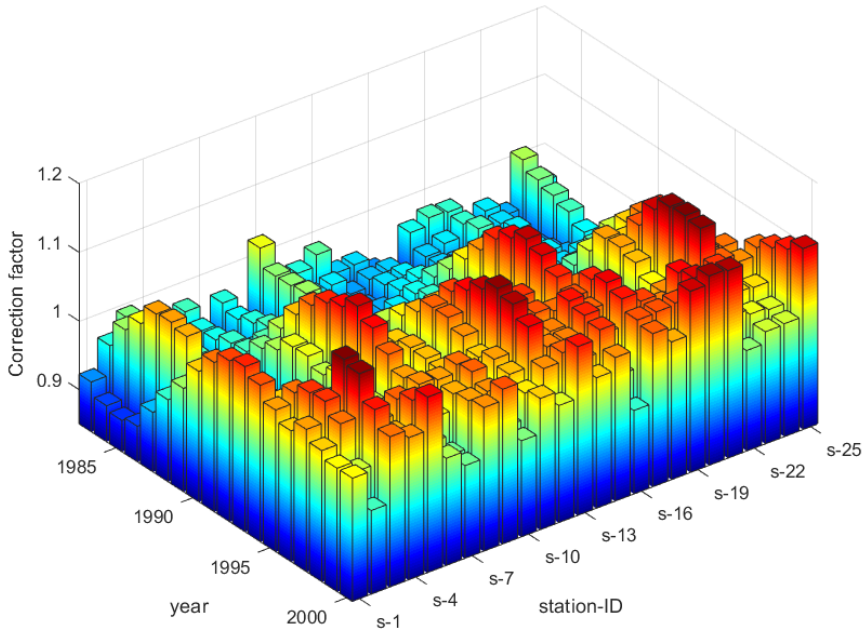


Figure 13. Matrix of correction coefficients for the conversion of the third subcycle (6 years) to the first major cycle (23 years).

4.4. Spatial Spread of the Conversion Coefficient and Analysis of Potential Influencing Factors

The above was done to calculate the annual average conversion coefficients of D20 and E601 evaporation pans for 158 meteorological stations in the Yangtze River Basin, and to spread them to the Yangtze River Basin by interpolation of the cubic spline function (Figure 14). In addition, we selected some station data to carry out a multiple linear regression analysis of the conversion factor and the meteorological influence factor, and to study the factors influencing the change in the spatial pattern of the conversion factor.

The average annual conversion factors for D20 and E601 pans in the Yangtze River Basin are basically in the range of 0.53–0.80. From the figure, we can see that the conversion coefficient of the Jinsha River Basin in the upper reaches of the Yangtze River Basin is generally small, around 0.55; the conversion coefficients of the Yalong River system, the Min River system, the Han River system and the Taihu Lake Basin are basically in the range of 0.55–0.70; and the conversion coefficients of the Jialing River system, the Wu River system, the Dongting Lake system and the Poyang Lake system are basically in the range of 0.65–0.80.

We attempted a multiple linear regression analysis between the conversion factors and meteorological factors, such as altitude, relative humidity, wind speed, sunshine duration, mean temperature, maximum temperature and minimum temperature using Stata software. Data from selected meteorological stations in the upper, middle and lower reaches of the Yangtze River Basin were selected separately. The regression coefficient results and significance levels are shown in Table 3. We found that the conversion factor was positively correlated with relative humidity, wind speed, minimum temperature and altitude; and negatively correlated with sunshine duration, average temperature and maximum temperature. The relationship between the conversion coefficient and meteorological factors is similar to the findings of Xu in the Yangtze River Basin [37], who found wind speed and relative humidity as significant factors influencing the spatial distribution pattern of the conversion coefficient; and found higher conversion coefficients, relatively higher humidity and relatively lower wind speed (compared to other regions) in the central part of the basin, which is consistent with our findings in the middle reaches of the Yangtze River Basin.

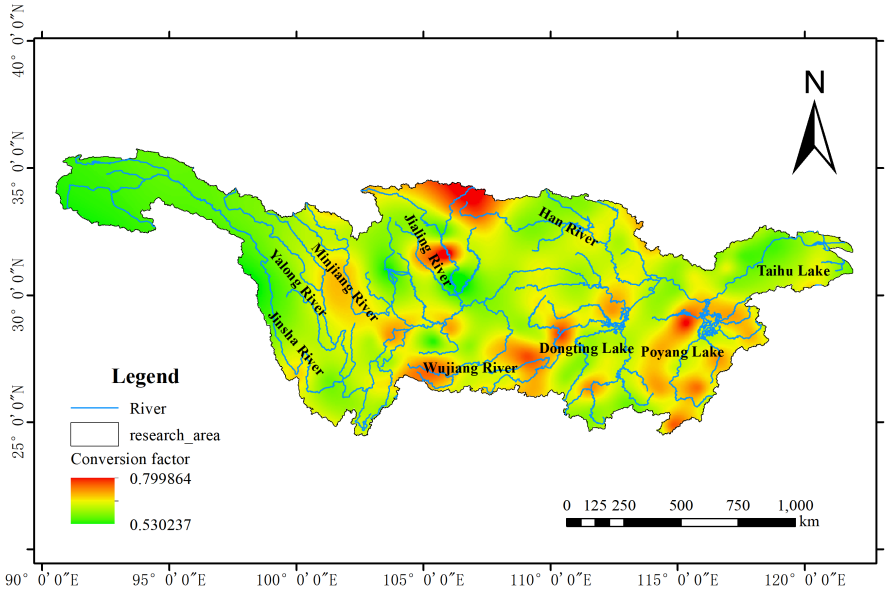


Figure 14. Spatial distribution of conversion coefficients for D20 and E601 pans in the Yangtze River Basin.

Table 3. Results of multiple linear regressions between conversion coefficients and climate factors. Hurs is relative humidity, Wind is wind speed, Sst is sunshine duration, Tave is mean temperature, Tmax is maximum temperature, Tmin is minimum temperature, Altit is altitude. Notes: standard errors in parentheses, *** $p < 0.01$, ** $p < 0.05$, * $p < 0.1$.

	Hurs	Wind	Sst	Tave	Tmax	Tmin	Altit
basin (n = 55,290)	0.0013 *** (−0.0002)	0.0226 *** (−0.001)	−0.0017 *** (−0.0005)	−0.0242 *** (−0.002)	−0.0029 *** (−0.0008)	0.0226 *** (−0.001)	1.7×10^{-5} *** (−0.0000)
56386 (n = 2972)	0.0019 *** (−0.0005)	0.0294 *** (−0.006)	−0.0036 ** (−0.002)	0.014 (−0.01)	−0.0207 *** (−0.006)	0.0008 (−0.005)	- -
56751 (n = 5584)	0.0042 *** (−0.0004)	0.001 (−0.003)	−0.013 *** (−0.002)	0.0207 *** (−0.005)	−0.0120 *** (−0.003)	−0.0115 *** (−0.003)	- -
57574 (n = 3723)	0.0015 (−0.001)	0.0547 *** (−0.011)	−0.0042 (−0.004)	−0.0472 ** (−0.02)	0.0024 (−0.01)	0.0401 *** (−0.01)	- -
57662 (n = 3968)	−0.00068 (−0.0005)	0.0034 (−0.006)	−0.0029 (−0.002)	−0.0300 *** (−0.01)	−0.00497 (−0.005)	0.0304 *** (−0.006)	- -
57707 (n = 3418)	−0.0019 ** (−0.0008)	0.0076 (−0.009)	−0.019 *** (−0.002)	0.0152 * (−0.008)	−0.0162 *** (−0.004)	0.0005 (−0.005)	- -
57866 (n = 3872)	0.00016 (−0.0005)	0.0173 *** (−0.004)	−0.0044 ** (−0.002)	−0.0338 *** (−0.009)	−0.0004 (−0.005)	0.0314 *** (−0.005)	- -
57972 (n = 3290)	−0.0032 *** (−0.0005)	−0.0239 *** (−0.003)	−0.0024 * (−0.001)	−0.0353 *** (−0.006)	0.0038 (−0.003)	0.0291 *** (−0.003)	- -
58238 (n = 5639)	0.0034 *** (−0.0005)	0.0570 *** (−0.003)	0.0026 * (−0.002)	−0.0337 *** (−0.007)	0.0023 (−0.004)	0.0231 *** (−0.004)	- -
58259 (n = 7120)	0.0016 *** (−0.0004)	−0.0026 (−0.003)	0.0012 (−0.001)	−0.0318 *** (−0.003)	−0.0019 ** (−0.0009)	0.0308 *** (−0.003)	- -
58519 (n = 5584)	0.00034 (−0.0005)	0.0584 *** (−0.004)	−0.0023 (−0.002)	0.0167 (−0.01)	−0.0217 *** (−0.006)	−0.0024 (−0.006)	- -
58637 (n = 4459)	−0.0024 *** (−0.0006)	0.0448 *** (−0.006)	−0.0049 ** (−0.002)	0.0174 ** (−0.009)	−0.0347 *** (−0.005)	0.0119 ** (−0.005)	- -
58813 (n = 5661)	−0.00036 (−0.0007)	0.0546 *** (−0.006)	0.0019 (−0.002)	0.00123 (−0.008)	−0.0181 *** (−0.004)	0.0102 ** (−0.005)	- -

The volume and depth of the water in the evaporation pan and its placement can also introduce uncertainty into the measured observations. The smaller size of the D20

pan, being 70 cm above the ground (Figure 1), and its relatively low specific heat capacity, resulted in a faster rise in water temperature in the D20 pan compared to the E601, which was buried in the soil and evaporated relatively steadily in comparison [30]; therefore, we could expect a negative correlation between the conversion coefficient and the average and maximum temperatures. When the temperature is low, due to the installation position being different and the volume of the water body being small, the D20 pan is in direct contact with the air. The temperature of the water body in the evaporation pan drops sharply with the temperature, to below 0 °C, the phenomenon of icing will occur, whereas the E601 pan would still be liquid. This gives rise to a possible positive correlation between the commutation coefficient and the minimum temperature.

As can be seen in Table 3, there is a negative correlation between sunshine duration and the conversion factor. This finding was also confirmed by previous studies [28,38]. Similarly, based on the energy balance experiment, the study found that the conversion coefficient between the type a evaporating pan and the water surface evaporation mainly depends on the additional radiation absorbed by the vessel wall [39]. As a result, the D20 pan absorbs radiation and transfers heat to the water, thereby increasing evaporation and reducing the conversion factor, whereas E601 pan is buried in the soil and is relatively unaffected.

In summary, factors such as altitude, relative humidity, wind speed, sunshine duration, average temperature, maximum temperature, minimum temperature and measuring instruments all affect the conversion coefficient of the evaporation pan, and the combination of these factors produces a change in the spatial pattern of the conversion coefficient. However, further capturing the specific effects of individual factors on the conversion factor requires rigorous experimental studies or more reasonable evaporation models [39,40].

4.5. Spatial Distribution of E601 Evaporation in the Basin

Pan evaporation observations do not reflect the evaporation physically happening at the Earth's surface. However, it serves as a useful proxy so that a standardized evaporation dataset with a long time series can be established, which is desirable for global change studies [22]. After 2001, when the D20 evaporation pan was gradually replaced in most areas, it was necessary to convert the D20 pan data to match the E601 pan data by using the conversion factors described above in order to make the historical data series compatible with the available data. In this study, the meteorological data from the D20 pan and the E601 pan were used as the basis, and the D20 pan data could be used as supplementary values for the missing data from the E601 pan. The data were combined using conversion factors, and some missing segments of the dataset were interpolated (see Section 3.2.5 for details) to finally create the E601 evaporation daily dataset, having a time series of 1980–2019 and 300 hydrological stations. In this paper, since the observations at the monitoring stations only represent small regional evaporation, the annual average water surface evaporation at the hydrological stations in the Yangtze River Basin was spread over the basin's space by interpolation of the spline function (Figure 15).

We can see that evaporation from the water's surface in the upper reaches of the Yangtze River Basin is on the high side, around 900–1500 mm; evaporation from the water's surface in the middle and lower reaches is less, around 500–1000 mm. The spatial pattern of mean annual evaporation is generally consistent with previous studies [24,41,42]. Among these, we the highest water evaporation has been reported for the southwest, reaching 1500 mm in most areas. By analyzing the spatial and temporal characteristics of wet and dry variability in the southwest from 1960 to 2009, studies have consistently found that drought events in the southwest have increased in intensity and frequency over the past half century due to a combination of decreasing precipitation and increasing temperatures [43,44]. Wang assessed potential changes in the framework of CMIP5 (Coupled Model Intercomparison Project Phase 5) in future droughts in southwest China [45]. By the end of the 21st century, water vapor transport in the Bay of Bengal had increased, temperatures had risen, net surface radiation had increased, relative humidity had decreased and precipitation and evaporation had tended to increase [46]. In view of the current impact and future threat

of the drought disaster in the southwest, it is imperative to propose water management solutions, restructuring of cultivation and soil conservation.

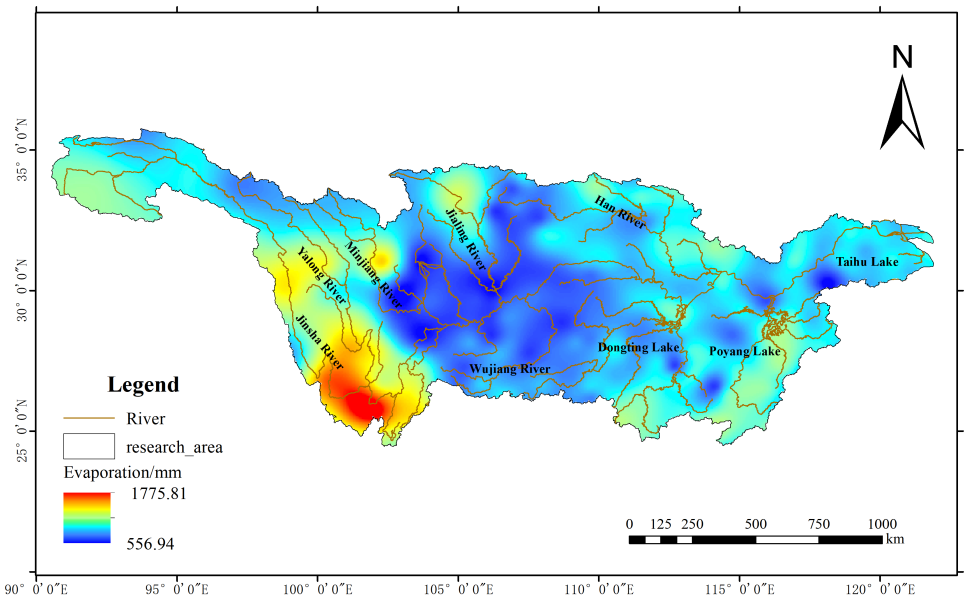


Figure 15. The spatial distribution of the reconstructed dataset for the E601 pan of the Yangtze River Basin.

5. Conclusions

This paper presented a governance and improvement method for dual-source evaporation data. Firstly, it involved extracting two types of evaporation data with good data integrity, sufficient series representation and consistent time series; then, the conversion coefficients of the two pans were used as a bridge to merge the dual-source data into single-source data; finally, the missing fragment data were interpolated using site data, nearby site correction porting and other methods for refinement. The method enables the homogenization of data from different evaporation observation series and is used to solve the problem of inconsistent and discontinuous station data. The method could be an interesting tool for hydrologists and environmentalists in regional hydrological calculations, water resource management and climate change patterns.

We practiced the application of data governance and enhancement methods in the Yangtze River Basin. Firstly, 25 stations with more complete evaporation data from D20 pan in the Yangtze River Basin were selected for wavelet periodicity analysis, and 23, 12 and 6 years were obtained as the first, second and third periods of the long series of evaporation data, respectively. Secondly, taking the observation data of the stations that meet the first cycle as a representative sample, the conversion relationship between the main and sub-cycles was studied, and the conversion coefficients of the two types of pans at the second and third cycle stations were corrected. The research result is that the revised value of the annual average conversion coefficient under the second cycle is 1.00427, and the revised value under the third cycle is 1.00564. Finally, the fusion and interpolation techniques of the dataset were carried out to create the daily dataset of evaporation from the E601 evaporation pan.

We spread the conversion coefficients of the two evaporation pans from the meteorological stations onto the basin and analyzed the potential influencing factors. We also built a daily evaporation dataset for the E601 evaporation pan of the Yangtze River Basin from 1980 to 2019 and spread it over the basin. The results of the study are as follows.

(1). The annual average conversion coefficients of D20 and E601 pans in the Yangtze River Basin are basically between 0.55 and 0.80, and there are obvious differences in different regions.

(2). The conversion coefficient was positively correlated with relative humidity, wind speed, minimum temperature and altitude; and negatively correlated with sunshine duration, mean temperature and maximum temperature.

(3). The water surface evaporation in the upper reaches of the Yangtze basin was on the high side, around 900–1500 mm; in the middle and lower reaches it was smaller, around 500–1000 mm. In particular, water surface evaporation was highest in the southwest—which has the greatest drought hazard—reaching 1500 mm in most areas.

In this paper, the spatial distribution map of the annual conversion coefficients of the D20 and E601 pans in the Yangtze River Basin was given in detail. The results can realize a convenient search for the conversion coefficients of the two evaporation pans in various regions of the Yangtze River Basin, and the rapid correction of the evaporation observation data of the local meteorological department to improve the quality of the data. The method can also be extended to the processing of other evaporation observation data in similar areas.

Author Contributions: Conceptualization, Z.L.; methodology, Z.L. and X.S.; software, Z.L.; validation, Y.Z.; formal analysis, S.Z.; investigation, Q.L.; data curation, Z.L.; writing—original draft preparation, Z.L.; writing—review and editing, Z.L.; project administration, X.S.; funding acquisition, X.S. All authors have read and agreed to the published version of the manuscript.

Funding: This study has been supported by the National Key Research and Development Program of China (2021YFC3200202), the China Three Gorges Corporation Research Project (Contract No: 202103044) and the Basic Research Project of China Institute of Water Resources and Hydropower Research (01882104, 01882106).

Institutional Review Board Statement: Not applicable.

Informed Consent Statement: Not applicable.

Data Availability Statement: All relevant data are available from an online repository or repositories (https://data.cma.cn/ accessed on 3 July 2022).

Conflicts of Interest: The authors declare no conflict of interest.

References

1. Wang, Y.; Jiang, T.; Xu, C. Study on the change trend of evaporation in the Yangtze River Basin from 1961 to 2000. *Clim. Chang. Res.* **2005**, *3*, 99–105.
2. Liu, J.; Cao, S.; Zhai, J. Trends and Influencing Factors of Pan evaporation in Shandong Province in Recent 50 Years. *J. Shandong Univ.* **2010**, *40*, 129–133. 138.
3. Peterson, T.C.; Easterling, D.R.; Karl, T.R.; Groisman, P.; Nicholls, N.; Plummer, N.; Torok, S.; Auer, I.; Boehm, R.; Gullett, D.; et al. Homogeneity adjustments ofin situ atmospheric climate data: A review. *Int. J. Climatol.* **1998**, *18*, 1493–1517. [CrossRef]
4. Roderick, M.L.; Hobbins, M.T.; Farquhar, G.D. Pan Evaporation Trends and the Terrestrial Water Balance. II. Energy Balance and Interpretation. *Geogr. Compass* **2009**, *3*, 761–781. [CrossRef]
5. Lim, W.H.; Roderick, M.L.; Farquhar, G.D. A mathematical model of pan evaporation under steady state conditions. *J. Hydrol.* **2016**, *540*, 641–658. [CrossRef]
6. Malik, A.; Kumar, A.; Kim, S. Modeling monthly pan evaporation process over the Indian central Himalayas: Application of multiple learning artificial intelligence model. *Eng. Appl. Comput. Fluid Mech.* **2020**, *14*, 323–338. [CrossRef]
7. Kisi, O.; Heddam, S. Evaporation modelling by heuristic regression approaches using only temperature data. *Hydrol. Sci. J.* **2019**, *64*, 653–672. [CrossRef]
8. Kushwaha, N.L.; Rajput, J.; Elbeltagi, A. Data Intelligence Model and Meta-Heuristic Algorithms-Based Pan Evaporation Modelling in Two Different Agro-Climatic Zones: A Case Study from Northern India. *Atmosphere* **2021**, *12*, 1654. [CrossRef]
9. Jin, L. Exploration of ice age water surface evaporation conversion factors and D20 water surface evaporator injection depths. *J. Libr. Inf. Sci.* **2003**, *01*, 144–145.
10. Zhang, Y. Overview of experimental research on water surface evaporation in China. *Yangtze River* **1999**, *03*, 7–9. 51.
11. Shen, D. Analysis of the data of E601B and E601 evaporators and 20 m^2 evaporation ponds. *J. China Hydrol.* **1999**, *03*, 33–36.
12. Wang, L.; Han, S.; Tian, F. Comparison of formulating apparent potential evaporation with pan measurements and Penman methods. *J. China Hydrol.* **2021**, *592*, 125816. [CrossRef]
13. Wang, K.; Dickinson, R.E.; Liang, S. Global Atmospheric Evaporative Demand over Land from 1973 to 2008. *J. Clim.* **2012**, *25*, 8353–8361. [CrossRef]

14. Brutsaert, W. Use of pan evaporation to estimate terrestrial evaporation trends: The case of the Tibetan Plateau. *Water Resour. Res.* **2013**, *49*, 3054–3058. [CrossRef]
15. Li, Z.; Chen, Y.; Shen, Y.; Liu, Y.; Zhang, S. Analysis of changing pan evaporation in the arid region of Northwest China. *Water Resour. Res.* **2013**, *49*, 2205–2212. [CrossRef]
16. Liu, Z.; Li, T. Global warming trend accelerates sharply. *Ecol. Econ.* **2019**, *35*, 1–4.
17. Pammar, L.; Deka, P.C. Daily pan evaporation modeling in climatically contrasting zones with hybridization of wavelet transform and support vector machines. *Paddy Water Environ.* **2017**, *15*, 711–722. [CrossRef]
18. Zhao, L.; Xia, J.; Xu, C. A review of evapotranspiration estimation methods in hydrological cycle simulation. *Acta Geogr. Sin.* **2013**, *68*, 127–136.
19. Guo, X.; Shi, J. Progress and trends in moisture evapotranspiration research at home and abroad. *Geol. Rev.* **2019**, *65*, 1473–1486.
20. Lu, Y.; Wang, Z.; Lv, H. Calculation of Water Surface Evaporation in Wudaogou Based on Principal Component Analysis and BP Neural Network *J. China Hydrol.* **2022**, *42*, 35–39.
21. Rotstayn, L.D.; Roderick, M.L.; Farquhar, G.D. A simple pan-evaporation model for analysis of climate simulations: Evaluation over Australia. *Geophys. Res. Lett.* **2006**, *33*. doi: 10.1029/2006GL027114. [CrossRef]
22. Xiong, A.; Liao, J.; Xu, B. Reconstruction of a Daily Large-Pan Evaporation Dataset over China. *J. Appl. Meteorol. Climatol.* **2012**, *51*, 1265–1275. [CrossRef]
23. Xu, Y.; Xu,Y.; Wang, Y.; Wu, L.; Li, G.; Song, S. Spatial and temporal trends of reference crop evapotranspiration and its influential variables in Yangtze River Delta, eastern China. *Theor. Appl. Climatol.* **2017**, *130*, 945–958. [CrossRef]
24. Wang, K.; Liu, X.; Li, Y.; Yang, X.; Bai, P.; Liu, C.; Chen, F. Deriving a long-term pan evaporation reanalysis dataset for two Chinese pan types. *J. Hydrol.* **2019**, *579*, 124162. [CrossRef]
25. Zuo, H.; Chen, B.; Wang, S.; Guo, Y.; Zuo, B.; Wu, L.; Gao, X. Observational study on complementary relationship between pan evaporation and actual evapotranspiration and its variation with pan type. *Agric. For. Meteorol.* **2016**, *222*, 1–9. [CrossRef]
26. Hu, S.; Tian, C.; Song, Y. Analysis of water surface evaporation conversion coefficients in the Tarim River basin. *J. Desert Res.* **2005**, *5*, 649–651.
27. Yang, L.; Meng, T.; Wu, D. Study on the conversion coefficients of different water surface evaporators in Maowusu sandy area. *Water Sav. Irrig.* **2021**, *311*, 55–59.
28. Fu, G.; Liu, C. Investigating the conversion coefficients for free water surface evaporation of different evaporation pans. *Hydrol. Process.* **2004**, *18*, 2247–2262. [CrossRef]
29. Sheng, Q.; Shen, S.; Gu, Z. Conversion factor of water surface evaporation for small evaporators. *Trans. Atmos. Sci.* **2007**, *119*, 561–565.
30. Li, Y.; Liu, C.; Liang, K. Spatial Patterns and Influence Factors of Conversion Coefficients between Two Typical Pan Evaporimeters in China. *Water* **2016**, *8*, 422. [CrossRef]
31. Cheong, W.K.; Timbal, B.; Golding, N.; Sirabaha, S.; Kwan, K.F.; Cinco, T.A.; Archevarahuprok, B.; Vo, V.H.; Gunawan, D.; Han, S. Observed and modelled temperature and precipitation extremes over Southeast Asia from 1972 to 2010. *Int. J. Climatol.* **2018**, *38*, 3013–3027. [CrossRef]
32. Li, J.; Wang, J.; Zhang, J.; Zhang, J.; Kong, H. Dynamic changes of vegetation coverage in China-Myanmar economic corridor over the past 20 years. *Int. J. Appl. Earth Obs. Geoinf.* **2021**, *102*, 102378. [CrossRef]
33. Li, L.; Wu, X.; Zhou, X. Characterization of river runoff evolution in coal mining areas based on Morlet wavelet theory. *Water Resour. Power* **2022**, *40*, 37–40.
34. Ogurtsov, M. A Study on Possible Solar Influence on the Climate of the Southern Hemisphere. *Atmosphere* **2022**, *13*, 680. [CrossRef]
35. Xu, W.; Li, Q.; Wang, X.L.; Yang, S.; Cao, L.; Feng, Y. Homogenization of Chinese daily surface air temperatures and analysis of trends in the extreme temperature indices. *J. Geophys. Res. Atmos.* **2013**, *118*, 9708–9720. [CrossRef]
36. Domonkos, P. Combination of Using Pairwise Comparisons and Composite Reference Series: A New Approach in the Homogenization of Climatic Time Series with ACMANT. *Atmosphere* **2021**, *12*, 1134. [CrossRef]
37. Xu, C.; Gong, L.Analysis of spatial distribution and temporal trend of reference evapotranspiration and pan evaporation in Changjiang (Yangtze River) catchment *J. Hydrol.* **2006**, *327*, 81–93. [CrossRef]
38. Yu, S.L.; Brutsaert, W. Evaporation from very shallow pans. *J. Appl. Meteorol. Climatol.* **1967**, *6*, 265–271. [CrossRef]
39. Lim, W.H.; Roderick, M.L.; Hobbins, M.T.; Wong, S.C.; Farquhar, G.D. The energy balance of a US Class A evaporation pan. *Agric. For. Meteorol.* **2013**, *182–183*, 314–331. [CrossRef]
40. Singh, V.P.; Xu, C.Y. Evaluation and generalization of 13 mass-transfer equations for determining free water evaporation. *Hydrol. Process.* **1997**, *11*, 311–323. [CrossRef]
41. Zuo, H.; Li, D.; Hu, Y.; Bao, Y.; Lü, S. Characteristics of climatic trends and correlation between pan-evaporation and environmental factors in the last 40 years over China. *Chin. Sci. Bull.* **2005**, *50*, 1235–1241. [CrossRef]
42. Wang, M.; Zhang, Y.; Lu, Y.; Gong, X.; Gao, L. Detection and attribution of reference evapotranspiration change (1951–2020) in the Upper Yangtze River Basin of China. *J. Water Clim. Chang.* **2021**, *12*, 2624–2638. [CrossRef]
43. He, J.; Zhang, M.; Wang, P.; Wang, S.; Wang, X. Climate Characteristics of the Extreme Drought Events in Southwest China during Recent 50 Years. *Acta Geogr. Sin.* **2011**, *66*, 1179–1190.
44. Li, Y.; Ren, F.; Li, Y.; Wang, P.; Yan, H. Characteristics of the regional meteorological drought events in Southwest China during 1960–2010. *J. Meteorol. Res.* **2014**, *28*, 381–392. [CrossRef]

45. Wang, L.; Chen, W.; Zhou, W. Assessment of Future Drought in Southwest China Based on CMIP5 Multimodel Projections. *Adv. Atmos. Sci.* **2014**, *31*, 1035–1050. [CrossRef]
46. Lin, W.; Wen, C.; Wen, Z.; Gang, H. Drought in Southwest China: A review. *Atmos. Ocean. Sci. Lett.* **2015**, *8*, 339–344.